

Autoionization of high- l Ba $6p_{1/2}nl$ states

R. R. Jones and T. F. Gallagher

Department of Physics, University of Virginia, Charlottesville, Virginia 22901

(Received 17 March 1988)

The autoionization rates and energies of the Ba $6p_{1/2}nl$ states for $n = 11-13$ have been measured using a multistep laser-excitation technique. The excitation is via the bound $6snl$ states which are populated using an electric-field switching method that allows the selective population of the high-angular-momentum states. The results of the measurements indicate an n^{-3} dependence and a rapid decrease of the autoionization rates with l . For the lowest- l states studied here, $l=4$, the rates are $\approx 10^{11} \text{ s}^{-1}$. At $l \approx 8$ the autoionization rates fall below the radiative decay rate of $2 \times 10^8 \text{ s}^{-1}$. Autoionization rates larger than 10^{10} s^{-1} are obtained by direct measurements of spectral widths, while smaller rates are determined by a saturation-broadening technique. The autoionization rates are in agreement with calculations based on an nl electron in a hydrogenic orbit around a Ba^+ core.

I. INTRODUCTION

The autoionization of high-angular-momentum states is a process of intrinsic interest due to the relative simplicity and stability of these states and the intimate relation to the quantum defects of both bound and autoionizing states.¹⁻³ High-angular-momentum autoionizing states are also of practical importance due to their role in dielectronic recombination in plasmas.⁴ The total dielectronic recombination rate is the sum of recombination rates through all the energetically available intermediate autoionizing states. In the isolated resonance approximation, which is very accurate for high- l states, it is straightforward to show that the dielectronic recombination rate through each autoionizing state is the same if the autoionization rate exceeds the radiative decay rate.⁶ Therefore a reasonable approximation to the recombination rate is obtained by counting the states for which the above criterion is fulfilled.⁶ Due to the large statistical weight of the high-angular-momentum states it is evident that they play an important role, in spite of their relatively low autoionization rates. Precisely how important they are depends on how rapidly the autoionization rates decrease with l , and in particular, at what l they are equal to the radiative decay rates.

High- l Ba $6pnl$ autoionizing states have been observed previously using excitation schemes which employ angular-momentum mixing of the Rydberg electron by static or microwave fields^{7,8} or through atomic collisions.⁹ However, these methods allow little or no selectivity as to which l values are excited or to the number of l levels which are populated. To date there has been only one limited measurement of the l dependence of autoionization rates, of Sr $5pnl$ states,¹⁰ but no systematic measurements which can serve to validate theoretical calculations of autoionization rates have been made. Here we present measurements of the autoionization rates of the Ba $6p_{1/2}nl$ states for $n = 11-13$ and $l = 4$ to $n-1$. These measurements are made using a three-step laser-excitation technique in conjunction with a Stark switch-

ing technique that allows us to circumvent the dipole selection rule and populate single high- l states. The observed autoionization rates are compared to calculations of the rates based on the model of an outer electron in a hydrogenic nl orbit circulating about a Ba^+ ion core. Since the calculated and measured rates are in reasonably good accord we conclude that this approach is adequate for such calculations.

In the following sections we describe our experimental approach, the observations, and the comparison with the calculations. We conclude with a few remarks concerning the implications for dielectronic recombination.

II. EXPERIMENTAL APPROACH

The laser excitation process, shown in Fig. 1, is similar to schemes described elsewhere,^{10,11} the only complica-

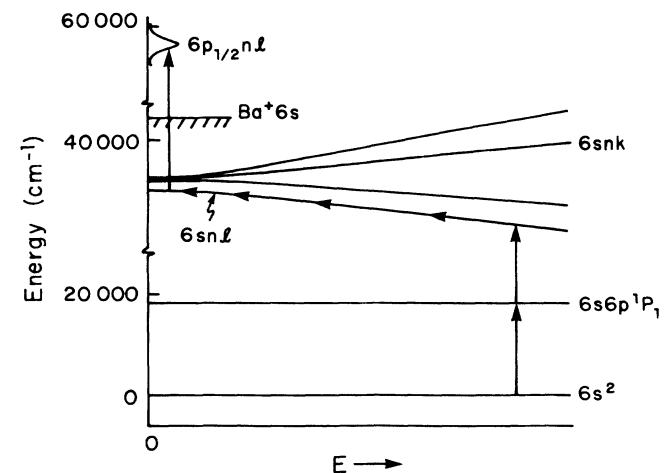


FIG. 1. Diagram of the combined laser excitation and electric-field switching process used to populate Ba $6p_{1/2}nl$ autoionizing states. First, two dye lasers are used to excite a $6snk$ level in a strong electric field. The field is then reduced adiabatically to zero and a third dye laser is used to excite the autoionizing level.

tion being the Stark switching technique. Two small dye lasers of the Hansch¹² type are used to populate, via the $6s6p\ ^1P_1$ state, a $6snk$ Rydberg-Stark state in a field of a few kV/cm. The field is then reduced to zero slowly enough that the $6snk$ atom passes adiabatically to a single $6snl$ state in zero field. At this point, a third, commercial dye laser is used to excite the autoionizing $6p_{1/2}nl$ state. The autoionizing resonances are observed by scanning the third laser over the $6snl-6p_{1/2}nl$ transition, which is near the $6s_{1/2}-6p_{1/2}$ Ba⁺ line at $20\,262\text{ cm}^{-1}$.¹³

The first small dye laser is pumped by the second harmonic of a Nd:YAG laser at 532 nm and is tuned to the $6s6p\ ^1P_1$ resonance at $18\,060\text{ cm}^{-1}$. The second Hansch laser is pumped by the third harmonic of the Nd:YAG laser at 355 nm and is used to excite the atoms to the $n=11-13$ levels (see Fig. 2) over the range $22\,800-24\,000\text{ cm}^{-1}$. Both of these lasers have linewidths of approximately 1 cm^{-1} and pulse lengths of 5 ns. The second laser is delayed after the first by 4 ns to ensure that the $6s6p$ resonance has been saturated before the appearance of the second laser. The commercial dye laser is pumped by an excimer laser operating with XeCl at 308 nm. The pulse length of the third laser is nearly 15 ns and has a linewidth of 0.05 cm^{-1} after the installation of an intracavity etalon. All three dye lasers are linearly polarized in the same direction, are pumped at a repetition of 20 Hz, and have pulse energies on the order of $100\ \mu\text{J}$.

The Ba atoms are excited in an effusive beam originating from a resistively heated oven in a vacuum chamber with a background pressure of 10^{-7} Torr. The Ba beam has a divergence of 15° and a density of approximately 10^9 atoms/cm³ at the interaction region, which is a distance of 15 cm from the oven. All three laser beams are

sent into the chamber collinear with each other and the atomic beam, but antiparallel to the atomic beam. The atomic beam and lasers overlap between a set of parallel aluminum field plates which are separated by a distance of 0.475 cm. After the Ba atoms autoionize, the ions are extracted through a group of 0.5-mm holes which are centered on the top plate in a circular area of 1 cm diam. A dual microchannel plate detector is centered 10 cm above the top field plate in order to measure the ion current from the interaction region. The signal from the microchannel plates is directed to a gated integrator where the signal is averaged and then recorded on an $x-y$ chart recorder.

As has been explained by others who have used similar excitation schemes previously,^{10,11} the final step in the excitation scheme, $6snl-6p_{1/2}nl$, is the strong Ba⁺ $6s-6p_{1/2}$ resonance line of the inner electron with the outer nl electron remaining as a spectator. This leads to excitation of the bound autoionizing state only, with no observable direct excitation to the continuum. Thus, no interference between bound and continuum channels occurs, and the location and width of the autoionizing state are readily observable by scanning the third dye laser over the $6snl-6p_{1/2}nl$ transition near the ion resonance line.

In zero field, the excitation $6s6p-6snl$ only allows $l=0$ or $l=2$ in the dipole approximation. In nonzero fields, however, any member of the Stark manifold corresponding to a given n may be excited due to the finite amount of s and d character in every state of the manifold. The Stark switching technique consists of exciting a given level of a Stark manifold in a strong electric field using the first two dye lasers. The field is then reduced adiabatically to zero field, and the excited state now only has the character of a single angular-momentum eigenstate. The

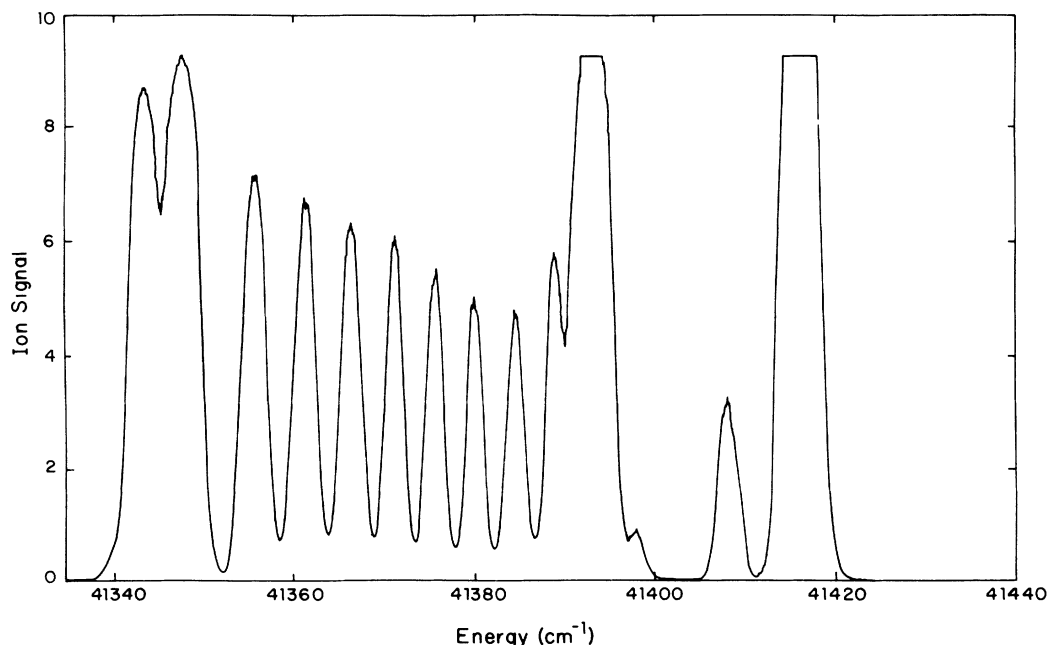


FIG 2. Scan of the second dye laser frequency over the $n=13$ manifold in an electric field of 2100 V/cm. Similar scans were used to determine the correct laser frequency to excite a particular $6p_{1/2}nl$ state.

field relaxation is adiabatic if its decay rate is always much less than the energy spacings between adjacent Stark states.

In order to ensure that the slew rate of our field meets the adiabatic condition, we have calculated the quantum defects of high-angular-momentum states of Ba under the approximation that the quantum defects are due to dipole and quadrupole polarizations of the Ba^+ ion core by the Rydberg electron. The calculations have been made using the method of Freeman and Kleppner,¹⁴ and the dipole and quadrupole polarizabilities of Ba^+ determined from the energy spacings between high-angular-momentum Rydberg states of Ba measured by Gallagher *et al.*³ These quantum defects are then used to calculate the Stark energy levels as a function of field strength using the method of Zimmerman *et al.*¹⁵ The theoretical quantum defects are shown in Table I.

In Fig. 3(a) we show a typical Stark energy level diagram. The energy levels for all angular-momentum states with effective quantum number $n = 13$ are shown as a function of applied electric field. Figure 3(b) is a magnification of the high-angular-momentum levels near zero field. As an example of our excitation scheme, consider the energy level near the point labeled *A* in Fig. 3(a). This energy level is excited by firing the first two lasers in an electric field of 2100 V/cm, shown by the arrow in Fig. 3(a). The electric field is then reduced slowly so that the relaxing state never tunnels through to a neighboring energy level. At zero field [see point *B* in Fig. 3(b)] the third laser is fired to excite the $6p_{1/2}nl$ autoionizing state.

For the range of states studied, fields up to 5000 V/cm are necessary to mix enough *s* and *d* oscillator strength into the rest of the manifold for adequate results. These strong fields are relaxed slowly using a 6BK4B electron tube which can short large voltages to ground at rates from 0 to 500 V/ μ s. Thus, after the second laser has excited a certain Stark state the field is relaxed to zero before the third laser is fired. After the firing of the third

laser, a small voltage pushes the ions, which are formed by autoionization, through the holes in the top field plate toward the detector. It should be noted that there is a trade off in deciding the proper slew rate for the electric field. While slow slew rates are necessary to achieve the adiabatic condition described above, slew rates which are too slow are not desirable. Due to the finite lifetimes of the excited Rydberg states, the number of atoms left in the proper excited state when the third laser fires falls off exponentially with the delay between the second and third lasers. Furthermore, longer delay times increase the probability of transitions to other states due to blackbody radiation.¹⁶

III. EXPERIMENTAL RESULTS

When scanning the third laser over the autoionizing states, we have found that the delay between the second and third lasers is extremely critical in determining the shape of the excitation profile (see Fig. 4). Firing the third laser in fields of approximately 50 V/cm instead of zero field produces scans exhibiting many overlapping peaks instead of the single Lorentzian which is characteristic of an unperturbed autoionizing level. As suggested by Fig. 3(b), the appearance of several peaks in nonzero fields is clearly due to the fact that for the levels studied, the angular-momentum levels with $l > 5$ are well mixed for fields of approximately 20 V/cm. Therefore, the method we use to find the zero-field position for the third laser is to change its temporal position until a delay time is reached which exhibits strong excitation to only one state. Almost all scans show some deviation from single Lorentzian profiles due to the fact that the field in the interaction region can change by 5–10 V/cm during the 15 ns laser pulse. Furthermore, the excitation profiles are found to be cleaner for larger slew rates since these allow shorter delay times. We believe that these shorter delays decrease the probability of state mixing by blackbody radiation and consequently minimize excitation of unwanted levels.

We find that reasonable amounts of oscillator strength can be put into the inner Stark levels if the first two lasers are fired in fields of 4200, 3000, and 2100 V/cm for $n = 11, 12,$ and $13,$ respectively. Slew rates range from approximately 800 V/cm μ s for $n = 11$ to 200 V/cm μ s for $n = 13$. Faster slew rates are used for the larger fields for the reasons explained above.

The autoionization rates for a given state are taken to be the FWHM of the Lorentzian profile in the scan of the third laser. Ordinarily, the third laser is attenuated until the signal amplitude is linear with the laser power to ensure that the width measured is the actual width of the autoionizing state, with no saturation broadening. However, for the range of principal quantum number studied, the excitation profiles for $l > 6$ have approximately constant width of 2.5 GHz. This is simply the combined width of many instrumental broadenings, the major contributors being the laser linewidth of 1.5 GHz and the Doppler width of approximately 1 GHz. It is assumed that all such instrumental widths are Gaussian and must be added in quadrature.

TABLE I. Calculated quantum defects of the $6s_{1/2}nl$ Rydberg levels and $6p_{1/2}nl$ autoionizing levels. Also shown are the quantum defects of the $6p_{1/2}nl$ autoionizing states derived from the positions of these states and the calculated values for the Rydberg levels. Values listed for the $6p_{1/2}nl$ states are the average values for $n = 11-13$.

<i>l</i>	Quantum defects		
	6s (calc.)	$6p_{1/2}$ (expt.)	$6p_{1/2}$ (calc.)
5	0.016	−0.029	−0.021
6	0.006 6	−0.013	−0.008 6
7	0.003 0	−0.005 7	−0.004 0
8	0.001 6	−0.002 1	−0.002 1
9	0.000 85	−0.001 3	−0.001 1
10	0.000 48	−0.000 58	−0.000 63
11	0.000 29	−0.000 29	−0.000 38
12	0.000 18		−0.000 25

In order to measure widths less than the instrumental width, we use the method of Cooke *et al.*¹⁷ The method basically uses saturation broadening to increase the natural Lorentzian width of the given state to values much greater than the instrumental widths. The nonsaturated width can then be deduced from the measured width. In

using the technique, we assume that all the Rydberg atoms in the third laser beam are excited to an autoionizing state and that the population of the autoionizing state has completely decayed away during the length of the excitation pulse. We also assume no power broadening of the upper level due to Rabi flopping between levels.

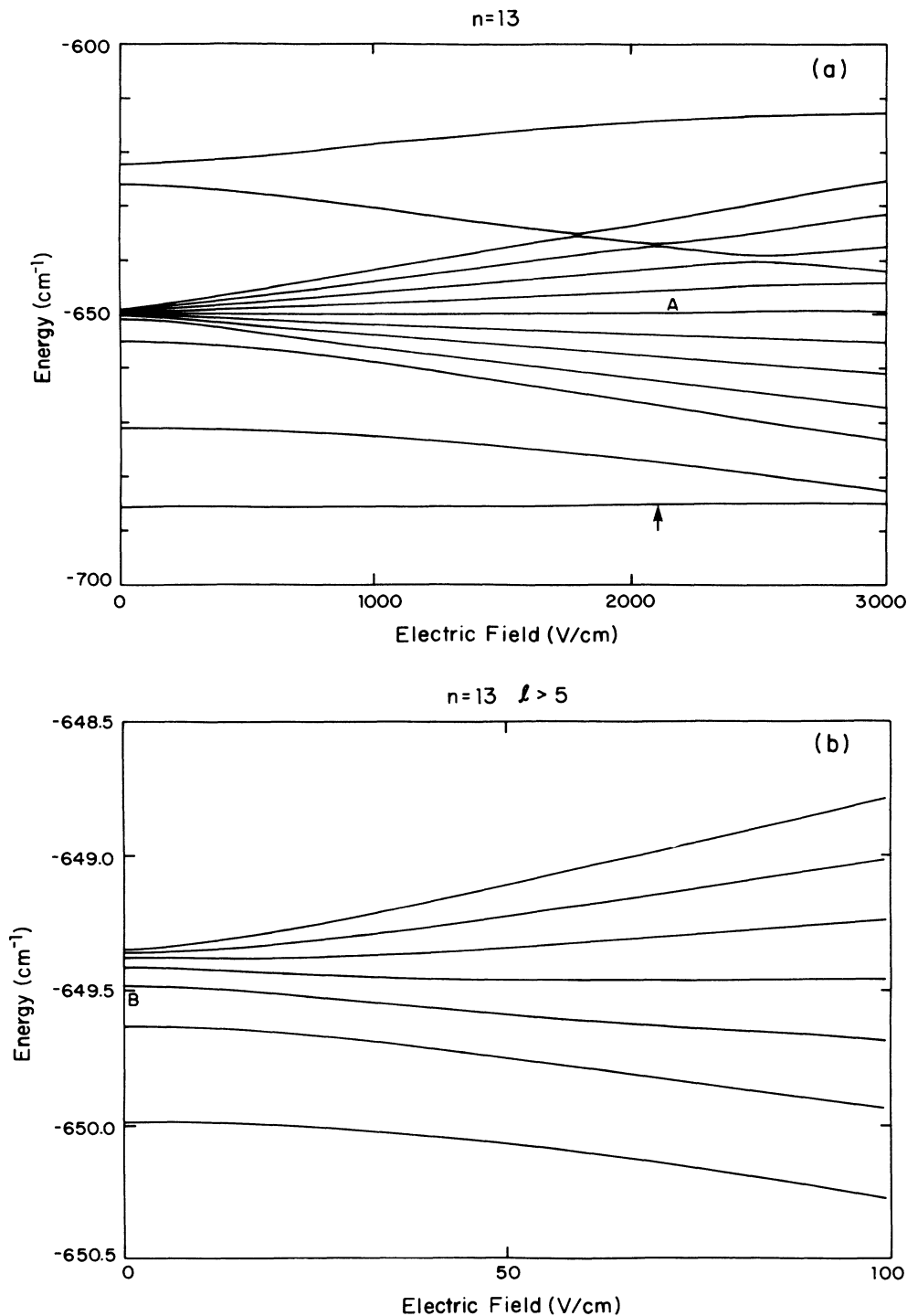


FIG. 3. (a) Calculated energy levels of the $n = 13$ Stark manifold as a function of applied electric field. The arrow indicates the field used to excite the $n = 13$ manifold when the data were taken. (b) Enlargement of the zero-field region in (a) which clearly shows the quadratic Stark shifts and quantum defects for the levels $l > 5$. The energy spacings of these states as the electric field approaches zero determine the maximum adiabatic slew rate.

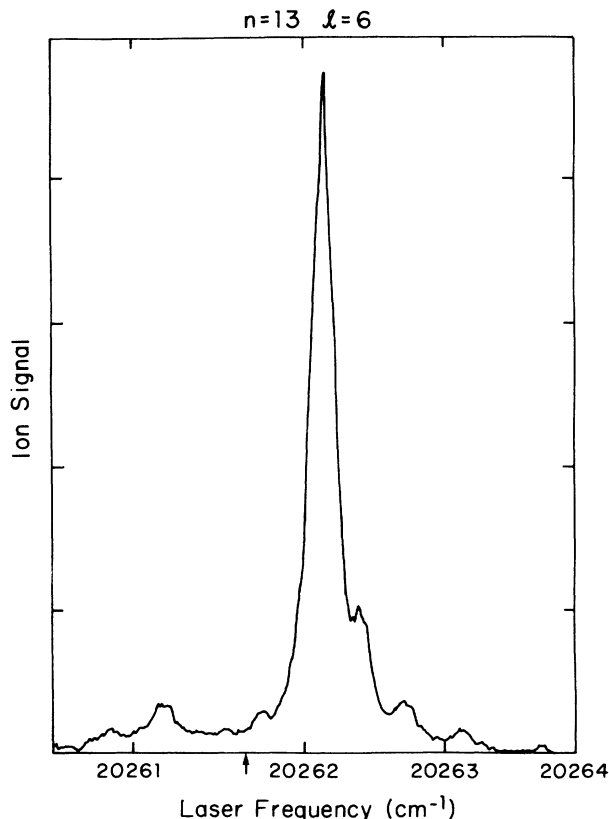


FIG. 4. Frequency scan of the third laser over the $\text{Ba}^+ 6s_{1/2}-6p_{1/2}$ transition line. This scan clearly exhibits strong excitation of the $6p_{1/2}13i$ autoionizing level and slight mixings with other levels. The ion line at 20261.6 cm^{-1} is also shown at the arrow.

These assumptions will be justified in the following sections.

The number of atoms driven to the excited autoionizing level in the saturation regime is given by

$$N = N_0(1 - e^{-\sigma\Phi}), \quad (1)$$

where σ is the excitation cross section and Φ is the time-integrated photon flux. The argument of the exponential in Eq. (1) can be written as

$$\sigma\Phi = \frac{\Gamma\tau\Omega^2}{\Delta\omega^2 + (\Gamma_N/2)^2}, \quad (2)$$

where Γ is the total decay rate of the upper state, τ is the laser pulse length, Ω is the dipole coupling between the upper and lower levels, $\Delta\omega$ is the detuning of the laser from the resonance line, and Γ_N is the observed width of the resonance including all instrumental broadenings. By comparing Eqs. (1) and (2) it is evident that $\sigma\Phi = \ln(2)$ when $2\Delta\omega$ is equal to the FWHM of the excitation profile. Thus, from Eq. (2) we have for two excited states 1 and 2 with the same dipole coupling from some lower states

$$\Gamma_1 = \frac{\Gamma_2(\Delta_1^2 + \Gamma_{N1}^2)}{\Delta_2^2 + \Gamma_{N2}^2}, \quad (3)$$

where Δ_1 and Δ_2 are the observed saturation-broadened

FWHM of states 1 and 2, respectively. Therefore, if the actual width and broadened width of state 2 are known and the broadened width of state 1 is known, then the actual width of state 1 can be determined.

Since the final excitation of the autoionizing states is of the inner electron, the dipole coupling between the Rydberg and autoionizing levels is the same for any outer-electron configuration if the laser power is constant. Therefore, because we can measure the widths of the $l=5$ and 6 levels directly, we are able to determine the widths of those states with $l > 6$ by saturation broadening all the levels and using Eq. (3).

The measured widths for all the levels studied are listed in Table II and plotted in Fig. 5. Due to the short lifetime of the $6sng$ states, virtually no population is left in these states when the third laser is fired. We find sufficient signal for a legitimate measurement for the $6p_{13g}$ level only. The width we list here is in good agreement with the value of 3.23 cm^{-1} reported previously by Jaffe *et al.*¹⁸ Also, for $n=12$ and 13 we cannot find sufficient signal for a valid rate determination for the $l=n-1$ levels. Therefore, no measurements are listed for these two states.

The quantum defects for $6p_{1/2}nl$ states are derived from the relative positions of the measured levels with respect to the $\text{Ba}^+ 6s_{1/2}-6p_{1/2}$ ion transition and the calculated quantum defects for the $6s_{1/2}nl$ states. These quantum defects are listed in Table I and plotted in Fig. 6.

The measured rates we report here are actually the total decay rates of the $6p_{1/2}nl$ states. These decay rates approach the spontaneous radiative decay rate of the $\text{Ba}^+ 6p_{1/2}$ state for small autoionization rates. Figure 5 clearly exhibits this lower limit at 25.5 MHz.¹⁹ With this observation we can now justify the assumptions we made in order to use the broadening technique. First, the branching ratio from the $\text{Ba}^+ 6p_{1/2}$ state to the $5d_{3/2}$ state is 22%,¹⁹ and there are approximately three radiative lifetimes of the $6p_{1/2}$ state during each laser pulse. Since atoms appearing in a $5dnl$ state also autoionize, essentially every atom which is excited to a $6pnl$ state will autoionize through some channel, and the population of the $6pnl$ level will have decayed away during the laser pulse time. Furthermore, we may assume that there is no significant Rabi or power broadening since, for every n studied, the highest- l states are not significantly broadened above the instrumental width. Therefore, the power broadening for all the states studied is, at most, comparable to the instrumental width since the Rabi broadening is independent of the values of n and l of the Rydberg electron. Hence, the lower- l states which are saturation broadened significantly above the instrumental width can have no added width due to Rabi broadening. Finally, the fact that the data are consistent with the radiative rate for the highest- l states shows that Rabi broadening is not a significant part of these widths either.

IV. THEORETICAL TREATMENT

Our theoretical calculations of the autoionization widths are based on a simple model of a single Rydberg

TABLE II. Calculated and observed total decay rates of the $6p_{1/2}nl$ levels for $n = 11-13$ and $l = 4$ to $n - 1$.

$6p_{1/2}n,l$	Expt. width (cm^{-1})	Uncertainty (cm^{-1})	Theor. width (cm^{-1})
11, 5	0.82	0.02	1.7
11, 6	0.16	0.004	0.16
11, 7	0.017	0.002	0.011
11, 8	0.003 8	0.0004	0.001 3
11, 9	0.000 52	0.0003	0.000 86
11, 10	0.000 42	0.0003	0.000 85
12, 5	0.73	0.04	1.35
12, 6	0.11	0.01	0.14
12, 7	0.018	0.003	0.010
12, 8	0.001 7	0.0003	0.001 4
12, 9	0.000 91	0.0002	0.000 86
12, 10	0.000 98	0.0002	0.000 85
13, 4	2.63	0.07	7.2
13, 5	0.51	0.03	1.1
13, 6	0.11	0.004	0.12
13, 7	0.032	0.003	0.009 3
13, 8	0.011	0.002	0.001 4
13, 9	0.002 4	0.001	0.000 87
13, 10	0.001 3	0.0005	0.000 85
13, 11	0.002 0	0.0009	0.000 85

level interacting with a single continuum. Such a simple model is valid as long as the perturbation of the single level is much smaller than the separation of the level from the nearest member of its Rydberg series. If we denote V as the perturbation which connects a $6p_{1/2}nl$ level to the continuum, then the autoionization rate is given by²⁰

$$\Gamma = 2\pi |V|^2. \quad (4)$$

In our model the perturbing potential is simply the Coulomb repulsion of the outer electron from the inner electron and can be written

$$V = \left\langle 6p_{1/2}nJ \left| \frac{1}{r_{12}} \right| n'l'\epsilon l''J \right\rangle, \quad (5)$$

where r_{12} is the separation between the two electrons. In our case, $n'l'$ is either $6s_{1/2}$ or $5d_{3/2}$, ϵ is determined from the energy conservation, and the total rate is taken as the sum of the rates to the different continua. We assume that the total wave function of the two electrons is separable into a product of a Coulomb wave for the inner electron and a hydrogenic wave for the outer electron. The operator in Eq. (5) may be expanded in terms of spherical harmonics. Taking the dipole term as the dominant contribution, V can be approximated by

$$V = \left\langle 6p_{1/2}nJ \left| \frac{r_i}{r_0^2} \mathbf{C}_1^1 \cdot \mathbf{C}_2^1 \right| n'l'\epsilon l''J \right\rangle, \quad (6)$$

where r_i is the radial position of the inner electron and r_0

is the radial position of the outer electron. The angular parts of V are calculated using standard methods,²¹ and the radial integrals for the Rydberg electron are performed using Numerov integration. The matrix elements r_{6p6s} and r_{6p5d} are calculated using the method of Lindgard and Nielsen¹⁹ and are found to have the values $4.33a_0$ and $2.59a_0$, respectively. The calculations have been performed using jj - jj , jk - jk , and jk - jj coupling, but the results are found to be independent of the coupling scheme.

The theoretical values shown in Fig. 5 are the calculated autoionization rates described here for $J=l$ added to the total radiative rate of the Ba^+ $6p_{1/2}$ state. $J=l-1$ and $l+1$ are also allowed total angular-momentum values for the autoionizing states in our excitation scheme. However, in both jj and jk coupling, states with $J=l$ are twice as likely to occur as $J=l-1$ or $J=l+1$. We therefore assume that the large excitation features are due to the $J=l$ state. Inspection of Fig. 5 indicates that this simple model reproduces the experimental results relatively well.

An interesting, although not very surprising, result of our calculations is that the angular integrals are extremely insensitive to the angular momentum of the Rydberg electron for $l > 4$. Instead, the radial integrals from bound to continuum channels account for almost all the angular-momentum dependence of the rates. We note that the radial integrals for $l''=l-1$ are an order of magnitude smaller than those with $l''=l+1$ for all the states studied. Furthermore, our calculations show a marked decrease in the branching ratio of autoionization to $6s_{1/2}\epsilon l'$ as is shown in Table III. The ratios are listed in

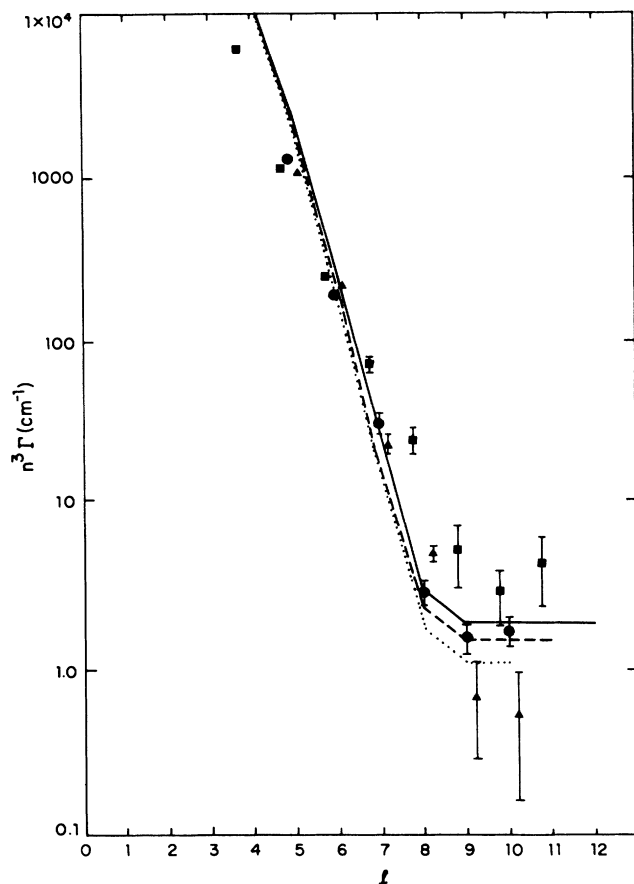


FIG. 5. Experimental and theoretical total decay rates of Ba $6p_{1/2}nl$ states. Calculated rates are shown as lines ($n=13$, —; $n=12$, ---; $n=11$, \cdots) for aesthetic reasons but were only calculated for integral values of l . The $n=13$ and $n=11$ data points are slightly shifted to the left and right of their correct positions, respectively, to prevent confusion due to overlapping points ($n=13$, \blacksquare ; $n=12$, \bullet ; $n=11$, \blacktriangle). Note the lower decay-rate limit of all the nl states at the spontaneous decay rate of the Ba^+ $6p_{1/2}$ level at 25.5 MHz.

Table III are very consistent for $n=11-13$ and $l=4-9$. However, our numerical calculations give values for the highest- l states which we believe to be spurious, and therefore, these values are not reported in Table III.

A simple second-order perturbation-theory calculation has been performed to determine the atomic energy shifts due to the perturbation in Eq. (6) with the $\epsilon l''$ autoionizing state replaced by an $n''l''$ Rydberg level. The quantum defects of the $6p_{1/2}nl$ states are readily obtainable

TABLE III. Calculated branching ratios for autoionization of $6p_{1/2}nl$ states to $6s_{1/2}\epsilon l$ and $5d_{3/2}\epsilon l$.

l	Branching ratios	
	$6s$ (%)	$5d_{3/2}$ (%)
4	43	57
5	38	62
6	32	68
7	27	73
8	22	78
9	18	82

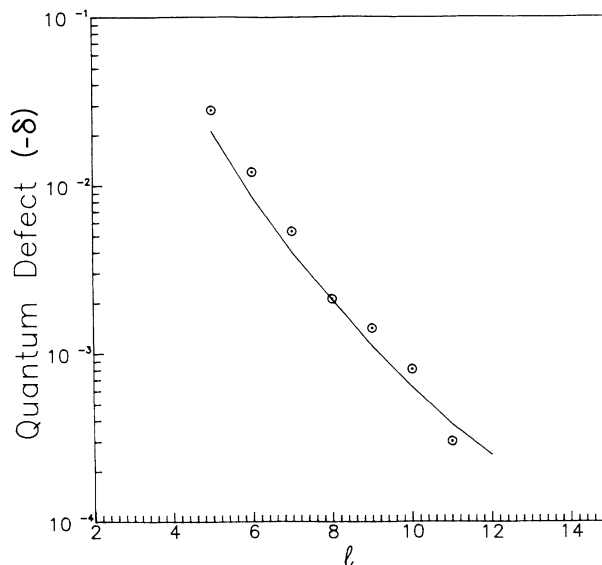


FIG. 6. Experimental and theoretical $6p_{1/2}nl$ quantum defects plotted vs l . The theoretical values are shown by the solid line, but calculations were only performed for integral values of l . Note that for all the levels studied, the quantum defects were found to be negative.

from these energy shifts. In the calculation, we assume that the only states of the inner electron which connect to the $6p_{1/2}$ state are the $6s_{1/2}$, $5d_{3/2}$, and $7s_{1/2}$ states. Furthermore, we assume that the energy interval $W_{6pnl} - W_{n'l'n''l''}$ has the constant value $W_{6p} - W_{n'l'}$ in order to use closure in the sum over the Rydberg electron states. The quantum defects we obtain by this method reproduce the measured values quite well and are listed in Table I and are plotted in Fig. 6. An interesting note is that the calculated and measured quantum defects have negative values. This observation may seem counterintuitive, but the negative quantum defects of the $6pnl$ states are a direct consequence of the positive quantum defect of the $6snl$ and $5dnl$ levels.

V. CONCLUSION

We present measurements of the total decay rates of Ba $6p_{1/2}nl$ autoionizing states for $n=11-13$ and $l=5$ to $n-1$. The decay rates are dominated by the autoionization process for $l < 8$, but radiative decay becomes dominant for $l > 8$. We use a simple theoretical model which reproduces our data within our experimental uncertainties. In the regime where the major channel is radiative we believe that autoionization still occurs through $5d_{3/2}nl$ states. It would be interesting to observe the shift in electron energies as low-energy autoionization becomes dominant. Unfortunately, the present measurement technique involves large electric fields which make electron-energy analysis impossible.

ACKNOWLEDGMENT

This work was supported by the U.S. Department of Energy, Office of Basic Energy Sciences, Division of Chemical Sciences.

- ¹W. E. Cooke and T. F. Gallagher, *Phys. Rev. A* **19**, 2151 (1979).
- ²J. H. Van Vleck and N. G. Whitelaw, *Phys. Rev.* **44**, 551 (1933).
- ³T. F. Gallagher, R. Kachru, and N. H. Tran, *Phys. Rev. A* **26**, 2611 (1982).
- ⁴V. L. Jacobs, J. Davis, and P. C. Kepple, *Phys. Rev. Lett.* **37**, 1390 (1976).
- ⁵M. J. Seaton and P. J. Storey, in *Atomic Processes and Applications*, edited by P. G. Burke and B. L. Moiseiwitsch (North-Holland, Amsterdam, 1977).
- ⁶D. C. Griffin, M. S. Pindzola, and C. Bottcher, *Phys. Rev. A* **31**, 568 (1985).
- ⁷S. M. Jaffe, R. Kachru, N. H. Tran, H. B. van Linden van den Heuvell, and T. F. Gallagher, *Phys. Rev. A* **30**, 1828 (1984).
- ⁸R. R. Jones and T. F. Gallagher (unpublished).
- ⁹F. Roussel, P. Breger, F. Gounand, and G. Spiess, *Europhys. Lett.* **5**, 309 (1988).
- ¹⁰W. E. Cooke, T. F. Gallagher, S. A. Edelstein, and R. M. Hill, *Phys. Rev. Lett.* **40**, 178 (1978).
- ¹¹N. H. Tran, P. Pillet, R. Kachru, and T. F. Gallagher, *Phys. Rev. A* **29**, 2640 (1984).
- ¹²T. W. Hansch, *Appl. Opt.* **11**, 895 (1972).
- ¹³C. E. Moore, *Atomic Energy Levels*, Natl. Bur. Stand. (U.S.) Circ. No. 467 (U.S. GPO, Washington, D. C., 1949), Vol. 3.
- ¹⁴R. R. Freeman and D. Kleppner, *Phys. Rev. A* **14**, 1614 (1976).
- ¹⁵M. L. Zimmerman, M. G. Littman, M. M. Kash, and D. Kleppner, *Phys. Rev. A* **20**, 2251 (1979).
- ¹⁶T. F. Gallagher and W. E. Cooke, *Phys. Rev. Lett.* **42**, 835 (1979).
- ¹⁷W. E. Cooke, S. A. Bhatti, and C. L. Cromer, *Opt. Lett.* **7**, 69 (1982).
- ¹⁸S. M. Jaffe, R. Kachru, H. B. van Linden van den Heuvell, and T. F. Gallagher, *Phys. Rev. A* **32**, 1480 (1985).
- ¹⁹A. Lindgard and S. E. Nielsen, *At. Data Nucl. Data Tables* **19**, 613 (1977).
- ²⁰U. Fano, *Phys. Rev.* **124**, 1866 (1961).
- ²¹A. R. Edmonds, *Angular Momentum in Quantum Mechanics* (Princeton University Press, Princeton, NJ, 1960).